Characterisation and prion transmission study in mice with genetic reduction of sporadic Creutzfeldt-Jakob Disease risk gene *Stx6*

Short title: Prion disease and *Stx6* expression in mice

Emma Jones[1¶], Elizabeth Hill[1¶], Jacqueline Linehan[1], Tamsin Nazari[1], Adam Caulder[2], Gemma F Codner[2], Marie Hutchison[2], Matthew Mackenzie[2], Michael Farmer[1], Thomas Coysh[1], Michael Wiggins De Oliveira[1], Huda Al-Doujaily[1], Malin Sandberg[1], Emmanuelle Viré[1], Thomas J Cunningham[1], Emmanuel A Asante[1£], Sebastian Brandner[3], John Collinge[1], Simon Mead[1*]

[1] Medical Research Council Prion Unit at University College London (UCL), UCL Institute of Prion Diseases, London W1W 7FF, United Kingdom

[2] Mary Lyon Centre at MRC Harwell, Harwell Campus, Oxfordshire OX11 0RD, UK

[3] Division of Neuropathology and Department of Neurodegenerative Disease, UCL Queen Square Institute of Neurology, Queen Square, London, WC1N 3BG, UK.

[¶] These authors contributed equally to this work

[£] Present address: AsanSka University College of Design and Technology, P.O. Box VV 179, Oyibi, Ghana

[*] To whom correspondence may be addressed. Email: s.mead@prion.ucl.ac.uk

Abstract

Sporadic Creutzfeldt-Jakob disease (sCJD), the most common human prion disease, is thought to occur when the cellular prion protein (PrP^C) spontaneously misfolds and assembles into prion fibrils, culminating in fatal neurodegeneration. In a genome-wide association study of sCJD, we recently identified risk variants in and around the gene *STX6*, with evidence to suggest a causal increase of *STX6* expression in disease-relevant brain regions. *STX6* encodes syntaxin-6, a SNARE protein primarily involved in early endosome to *trans*-Golgi network retrograde transport. Here we developed and characterised a mouse model with genetic depletion of *Stx6* and investigated a causal role of *Stx6* expression in mouse prion disease through a classical prion transmission study, assessing the impact of homozygous and heterozygous syntaxin-6 knockout on disease incubation periods and prion-related neuropathology. Following inoculation with RML prions, incubation periods in *Stx6*$^{-/-}$ and *Stx6*$^{+/-}$ mice differed by 12 days relative to wildtype. Similarly, in *Stx6*$^{-/-}$ mice, disease incubation periods following inoculation with ME7 prions also differed by 12 days. Histopathological analysis revealed a modest increase in astrogliosis in ME7-inoculated *Stx6*$^{-/-}$ animals and a variable effect of *Stx6* expression on microglia activation, however no differences in neuronal loss, spongiform change or PrP deposition were observed at endpoint. Importantly, *Stx6*$^{-/-}$ mice are viable and fertile with no gross impairments on a range of neurological, biochemical, histological and skeletal structure tests. Our results provide some support for a pathological role of *Stx6* expression in prion disease, which warrants further investigation in the context of prion disease but also other neurodegenerative diseases considering syntaxin-6 appears to have pleiotropic risk effects in progressive supranuclear palsy and Alzheimer's disease.

Author Summary

Sporadic Creutzfeldt-Jakob disease (sCJD), the most common human prion disease, is an invariably fatal disease with no established disease-modifying treatments. The identification of *STX6* as a proposed risk gene for sCJD motivated the generation of a new mouse knockout model, in which we found no grossly deleterious phenotypes. A transmission study in *Stx6*$^{-/-}$, *Stx6*$^{+/-}$ and *Stx6*$^{+/+}$ mice challenged with two prion strains showed reduced syntaxin-6 expression is associated with a modest prolongation of prion disease incubation periods, supporting a pathological role of *Stx6* expression in prion disease pathogenesis. Syntaxin-6 appears to have pleiotropic risk effects across multiple neurodegenerative diseases including progressive supranuclear palsy and Alzheimer's disease. Thus, this work supports further exploration of the *STX6* susceptibility mechanism, which likely has relevance across multiple neurodegenerative diseases.

Introduction

Prion diseases are transmissible neurodegenerative conditions of humans and animals with no established treatments. The infectious agent of prion diseases, or prion, comprises amyloid assemblies of misfolded host prion protein in a parallel in-register beta sheet conformation(1, 2). Sporadic Creutzfeldt-Jakob disease (sCJD), the most common human prion disease, invariably results in fatal neurodegeneration. sCJD is thought to result from the spontaneous formation of prions in the body by misfolding and aggregation of the host-encoded prion protein (PrP^C), triggering a self-perpetuating cycle whereby prion fibrils elongate by recruitment of cellular PrP with subsequent fission producing more infectious particles. Variation in the *PRNP* gene encoding PrP^C is a key genetic determinant of sCJD risk and phenotype, however there is now robust evidence for two non-*PRNP* genetic risk factors identified through a genome-wide association study. This study found a genetic region including *STX6* as a novel risk locus in human sCJD(3). Interestingly the *STX6* locus has also been implicated in other neurodegenerative diseases, with the same genetic variants being associated with progressive supranuclear palsy (PSP)(4, 5) and increased syntaxin-6 protein expression being causally associated with Alzheimer's disease (AD)(6, 7), indicating this protein may play a pleiotropic role in neurodegeneration.

STX6 encodes syntaxin-6, a member of the SNARE (soluble N-ethylmaleimide-sensitive factor attachment protein receptor) protein family, which is involved in the final step of membrane fusion during vesicle transport. Syntaxin-6 has been shown to be primarily involved in vesicle fusion during retrograde transport between early endosomes and the *trans*-Golgi network(8, 9). Analysis of expression quantitative trait loci (eQTLs) at this site identified *cis*-acting variants which increase *STX6* expression in disease-relevant brain regions, particularly the putamen

and caudate nuclei, which are commonly found to be abnormal in diagnostic MRI brain studies in sCJD(10). These and other gene prioritisation analyses identify *STX6* as the causal gene driving the increased sCJD risk at this locus.

Experimental inoculation of mice with prions faithfully recapitulates the neuropathological hallmarks seen in human prion diseases, notably the propagation and deposition of PrP aggregates, spongiform degeneration, neuronal loss and widespread glial cell and immune activation(11, 12). Furthermore, it has been long recognised that prions exist as conformationally distinct strains(13), which alter the disease progression and pathology in mice in a similar manner to human diseases. Prion strains RML and ME7 have been developed, whereby prions originally derived from sheep and goat scrapie have been serially passaged in mice resulting in mouse-adapted prions with high attack rates and well-defined incubation periods in a laboratory setting(11, 14). Mouse bioassay has been routinely used to measure prion infectivity(15, 16), as well as to further understand disease modifiers in a mammalian biological system(17, 18). In a standard experiment, the time from inoculation to prion disease diagnosis (termed “incubation period”) is the defining measure.

To explore a role for *Stx6* expression in prion disease pathogenesis, we conducted a classical prion transmission study in a newly developed mouse model which has a genetic reduction in *Stx6* expression. We show that knockout of syntaxin-6 does not result in a deleterious phenotype but had a 12 day longer incubation period following inoculation with RML or ME7 mouse-adapted scrapie prions, representing an 8% and 7% increase in the incubation periods relative to wildtype controls respectively. *Stx6*$^{+/-}$ mice showed an 8% prolongation of incubation periods following RML inoculation, although no extension in the incubation period was seen with ME7-inoculated *Stx6*$^{+/-}$ animals. No differences in neuronal loss, spongiform

101 change or PrP deposition were seen between the genotypes, however a variable effect of *Stx6*
102 expression on gliosis was observed at endpoint. This work provides complimentary evidence
103 that altered expression of *Stx6* modifies prion disease pathogenesis and supports the further
104 exploration of the functional role of syntaxin-6 in prion disease and related tauopathies.

105

106 ## Results

107 Generation of *Stx6* knockout C57BL/6N mice

108 We generated mice with homozygous deletion of *Stx6* (*Stx6*$^{-/-}$) on the C57BL/6N background
109 as part of the International Mouse Phenotyping Consortium(19) (IMPC) via CRISPR/Cas9-
110 mediated deletion of 1808 nucleotides spanning two critical exons (exons 6 and 7 of
111 transcripts *Stx6-201* and *Stx6-209* as depicted in **Fig 1A**, present within all protein coding
112 isoforms) replaced by an 8 nucleotide insertion, generating a premature stop codon.
113 Quantitative immunoblotting of whole brain homogenates demonstrated the loss of the
114 primary protein product at ~32 kDa in mice with homozygous deletion of *Stx6* (*Stx6*$^{-/-}$), whilst
115 heterozygous mice (*Stx6*$^{+/-}$) expressed ~50% of the protein compared to wildtype animals
116 (*Stx6*$^{+/+}$) (*Stx6*$^{-/-}$: 0.0757% ± 0.0217 (mean ± SEM); *Stx6*$^{+/-}$: 55.9% ± 0.0436) (**Fig 1B-C**). This was
117 also seen with an N-terminal syntaxin-6 antibody (**Error! Reference source not found.**).
118 Reduced expression of PrP^{C} has previously been shown to extend the incubation period in
119 mice(20). Therefore to determine any differences associated with *Stx6* expression, brain PrP^{C}
120 levels were assessed by enzyme-linked immunosorbent assay (ELISA). This analysis did not
121 reveal any differences in PrP^{C} expression with *Stx6* genotype (*Stx6*$^{+/+}$: 6115 ± 838.3 RFU (mean
122 ± SEM); *Stx6*$^{+/-}$: 5784 ± 1100 RFU; *Stx6*$^{-/-}$: 5834 ± 153 RFU) (**Fig 1D**).

123 *Stx6*$^{-/-}$ mice are physiologically normal

124 To determine any gross changes in organ morphology associated with altered *Stx6* expression,
125 immunohistochemical analysis was performed on liver, pancreas, kidney, skeletal muscle and
126 adipose tissue dissected from 4-5 adult mice (4 x *Stx6*$^{-/-}$, 5 x *Stx6*$^{+/-}$, 5 x *Stx6*$^{+/+}$, see Materials
127 and Methods). As shown in **Fig 2**, there were no differences in the appearance and

128 architecture between any tissue from *Stx6*$^{-/-}$, *Stx6*$^{+/-}$ and *Stx6*$^{+/+}$ animals aside from moderate
129 liver steatosis in one *Stx6* null animal, however as this was only found in one animal it is
130 unlikely to be related to the loss of *Stx6* expression (**Error! Reference source not found.**).
131 Furthermore, analysis of skeletal structure by computed tomography (CT) scanning did not
132 reveal any obvious differences in bone or skeleton architecture between genotypes (**Error!**
133 **Reference source not found.**).

134 Upon generation, *Stx6*$^{-/-}$ mice were subject to the standard IMPC phenotyping program at
135 MRC Harwell(21) (www.mousephenotype.org). This analysis suggested alterations in some
136 blood clinical chemistry parameters including increased blood urea nitrogen in early adult
137 females and increased circulating alkaline phosphatase in early adult males, but these findings
138 were not replicated in our independent sample ($P > 0.01$) (**Error! Reference source not**
139 **found.**, **Error! Reference source not found.**). The lack of replication or significance of these
140 phenotypes in other sexes or life stages indicates these perturbations are not replicable or
141 generalisable. In a pilot study, aged mice were examined on a range of behavioural and motor
142 tasks, including nest building, rotarod, grip strength, pellets burrowed and weight of food
143 consumed, with *Stx6*$^{-/-}$ and *Stx6*$^{+/-}$ (n = 5 per group) broadly comparable with wild-type
144 animals (the study was not powered to detect subtle differences in behaviours). Overall,
145 reduction in *Stx6* expression did not lead to a detectable deleterious phenotype in these
146 animals.

147 Mice with genetic reduction of *Stx6* have differing incubation periods when infected with two
148 mouse-adapted prion strains

149 To determine the effect of *Stx6* expression on the incubation period of prion disease, *Stx6*$^{-/-}$,
150 *Stx6*$^{+/-}$ and *Stx6*$^{+/+}$ female mice were inoculated intracerebrally with two mouse-adapted

151 scrapie prion strains, RML and ME7, or PBS as a vehicle control. An overall log-rank test of the
152 association of disease incubation period with *Stx6* genotype demonstrated a significant
153 relationship in both RML (P = 0.0049, **Fig 3A**) and ME7 (P < 0.0001, **Fig 3C**) inoculated animals,
154 suggesting *Stx6* expression modulates the incubation period of prion disease with both prion
155 strains.

156 To quantify these effects and define associations with specific genotypes, a secondary analysis
157 was performed looking at the differences between partial and complete genetic reduction in
158 *Stx6* expression for each strain (**Table 1**). Following inoculation with RML prions, the
159 incubation period in *Stx6*$^{-/-}$ and *Stx6*$^{+/-}$ mice differed by 12 days relative to wildtype animals
160 although statistical significance was only reached for *Stx6*$^{+/-}$ animals (*Stx6*$^{+/+}$ = 147 days [144
161 – 161] (median [95% confidence interval]), *Stx6*$^{+/-}$ = 159 days [154 – 168], *Stx6*$^{-/-}$ = 159 days
162 [156 – 160]) (**Fig 3A**). Furthermore, as a number of animals were excluded from analysis due
163 to early loss from intercurrent illness (especially for ME7 inoculated animals; see Materials
164 and Methods and **Error! Reference source not found.**), the time from inoculation until onset
165 of the first scrapie symptom was analysed (previously used as an alternative measure of
166 incubation period(22)). There was no significant association of *Stx6* genotype with incubation
167 period by this measure following RML inoculation (P = 0.14, **Fig 3B**), although there was still a
168 modest, nominal increase in incubation period in *Stx6*$^{-/-}$ animals compared to *Stx6*$^{+/+}$ (*Stx6*$^{+/+}$
169 = 133 days [127 – 139] vs *Stx6*$^{-/-}$ = 138 days [133 – 141]; *Stx6*$^{+/-}$ = 132 days [129 – 141]).
170 Although this analysis allows for greater inclusion of animals who were succumbing to the
171 disease, identification of the first neurological symptom is typically a more variable
172 assessment which likely underpins the differences between these two analyses.

173 In ME7-inoculated animals, incubation period also differed by 12 days with complete loss of
174 *Stx6* compared to wildtype animals (*Stx6*$^{+/+}$ = 162 days [161 – 168]) vs *Stx6*$^{-/-}$ = 174 days [174
175 – NA], **Fig 3C**), however there was no increase seen with heterozygous *Stx6* expression with
176 this strain (*Stx6*$^{+/-}$: 158 days [155 – 160]). In the analysis of time until onset of first neurological
177 symptom, there was still a significant association of *Stx6* genotype (P < 0.0001, **Fig 3D**) with a
178 7-day increase in *Stx6*$^{-/-}$ mice compared to *Stx6*$^{+/+}$ animals (*Stx6*$^{+/+}$ = 147 days [146 – 150] vs
179 *Stx6*$^{-/-}$ = 154 days [153 – 160]). Again however there was no effect of partial *Stx6* expression
180 loss on this prion strain (*Stx6*$^{+/-}$ = 146 days [140 – 151]).

181 Although some of the post-hoc pairwise comparisons demonstrating benefit with genetic
182 reduction of syntaxin-6 did not reach statistical significance (**Table 1**), the independent,
183 repeated observations of extended incubation period in *Stx6* knockout animals with two
184 distinct prion strains supports a general pathological role of expression of this gene in prion
185 disease progression. To explore whether *Stx6* exerts a selection effect for propagation of
186 distinct prion strains, we performed western blotting on end stage brain homogenates. This
187 demonstrated no change of PrP^{Sc} types with modified *Stx6* expression in either RML- or ME7-
188 inoculated animals as expected (**Error! Reference source not found.**).

Table 1: Summary of analysis for association of Stx6 genotype with disease incubation periods following inoculation with RML and ME7 prions.

		P*	Group	N start	N events	Median (days)	Lower 95% CI	Upper 95% CI	Diff. (vs WT) (days)	P (vs WT)**
Scrapie Clinical Diagnosis	**RML**	P = 0.0049	***WT***	*20*	*19*	*147*	*144*	*161*		
			HET	19	18	159	154	168	**+12**	0.0047
			KO	20	16	159	156	160	**+12**	0.17
	ME7	P < 0.0001	***WT***	*20*	*16*	*162*	*161*	*168*		
			HET	20	19	158	155	160	**-4**	0.00040
			KO	20	7	174	174	NA	**+12**	0.00075
First scrapie symptom	**RML**	P = 0.14	***WT***	*19*	*19*	*133*	*127*	*139*		
			HET	19	19	132	129	141	**-1**	0.86
			KO	20	20	138	133	141	**+5**	0.16
	ME7	P < 0.0001	***WT***	*20*	*18*	*147*	*146*	*150*		
			HET	20	19	146	140	151	**-1**	0.29
			KO	17	14	154	153	160	**+7**	1.20×10^{-7}

*Summary statistics for incubation periods measured as time until animals were culled once diagnostic clinical signs were noted (top) or onset of first scrapie-associated symptom (bottom) following intracerebral inoculation with 1% RML or ME7 infected C57BL/6 brain homogenate by Stx6 genotype (KO: $^{-/-}$; WT: $^{+/+}$; HET $^{+/-}$). Median incubation period in days listed with corresponding 95% confidence intervals. *P-value from overall log-rank test of Stx6 genotype with disease incubation period. **P-value from a pairwise log-rank test for association of each group with relative WT controls.*

197 Neuropathological features and *Stx6* expression

198 Prion disease is typically characterised by histological features of spongiform vacuolation,
199 neuronal loss and astrocyte proliferation(23), along with deposition of PrP aggregates in the
200 brain and a strong microglia response, which can be identified upon brain biopsy in patients,
201 or on post-mortem histopathological analysis of the brain in patients and animals(24).
202 Immunohistochemical staining with an anti-PrP antibody detected PrP deposits at the end-
203 stage of the disease following intracerebral inoculation with RML and ME7 prions in all
204 animals (7-10 mice analysed per group, see Materials and Methods) (**Fig 4**). With both prion
205 strains, disease-associated PrP can be detected with a diffuse staining pattern in grey matter
206 areas. In ME7-inoculated animals there was additional widespread deposition of micro-
207 plaques as previously described(24). At this resolution and time-point there was no difference
208 evident in appearance, extent or localisation of PrP aggregates between *Stx6* genotypes.

209 Considering this was the first characterisation of this mouse strain, we also assessed whether
210 manipulation of this genetic risk factor alone was sufficient to cause neuropathological
211 changes in the absence of prion infection. Knockout of *Stx6* did not cause detectable
212 deposition of disease-associated PrP in PBS-inoculated controls.

213 To determine whether there were any differences in spongiform vacuolation with *Stx6*
214 expression at endpoint, haematoxylin and eosin (H&E) staining was used to identify
215 morphological changes in the tissue. This analysis revealed the presence of distinct small,
216 round vacuoles within the neuropil in multiple brain regions including the striatum, cortex
217 and midbrain in prion-inoculated animals, reflecting the expected spongiform change
218 associated with these mouse prion strains (**Fig 5**). This analysis also showed the typical

219 neuronal loss within the hippocampus following ME7 inoculation. No changes were identified
220 in controls demonstrating knockout of *Stx6* alone does not induce pathological changes.

221 Taken together, these results provide further support for maintenance of prion strain type in
222 mice with genetic reduction of syntaxin-6, with no clear differences in PrP deposition patterns
223 and spongiform vacuolation between genotypes.

224 Possible increased inflammatory response with reduced *Stx6* expression

225 As widespread activation and proliferation of both astrocytes and microglia is a hallmark of
226 both human and animal prion disease, which progresses with disease duration,
227 immunohistochemical staining was performed to detect activated astrocytes and microglial
228 cells allowing quantification of any modulatory effects *Stx6* expression may have on
229 neuroinflammatory phenotypes in prion disease. Furthermore, control animals were analysed
230 to determine if *Stx6* knockout alone causes any inflammatory phenotypes.

231 Immunohistochemical staining of reactive astrocytes with an anti-GFAP antibody confirmed
232 the expected widespread astrocyte proliferation, with particular intensity in the thalamus and
233 hippocampus as previously described with these prion strains(25) (**Fig 6A**). Quantification of
234 mean percentage area shows >70% immunoreactivity in brain tissue under all prion-
235 inoculated conditions (ME7: $Stx6^{-/-}$ = 82.3% ± 0.820 (mean ± SEM), $Stx6^{+/-}$ = 71.7% ± 0.870,
236 $Stx6^{+/+}$ = 70.7% ± 2.15; RML: $Stx6^{-/-}$ = 79.2% ± 1.06, $Stx6^{+/-}$ = 82.6% ± 1.20, $Stx6^{+/+}$ = 78.6% ±
237 1.06) compared to ~40% in PBS-inoculated animals (PBS: $Stx6^{-/}$ = 42.4% ± 1.04, $Stx6^{+/-}$ = 44.3%
238 ± 0.630, $Stx6^{+/+}$ = 43.7% ± 0.478) (**Fig 6C**). This highlighted a ~10% increase in astrocyte area
239 in $Stx6^{-/-}$ mice inoculated with ME7 relative to both $Stx6^{+/-}$ (P_{adj} = 1.70 x 10^{-3}) and $Stx6^{+/+}$
240 animals (P_{adj} = 7.57 x 10^{-4}) after adjusting for age of death to take into account the later tissue

241 collection for the *Stx6*$^{-/-}$ mice with extended incubation periods. Of note, there was no
242 significant association between age and GFAP area stained. This highlights a potential
243 protective mechanism for reduced *Stx6* expression in prion diseases, for example if astrocytes
244 are acting to maintain neuronal function.

245 Immunostaining with an anti-Iba1 antibody to detect microgliosis demonstrated the expected
246 visible microglia activation following inoculation with both RML and ME7 prions, occupying
247 25-30% of the whole brain area in all disease conditions (ME7: *Stx6*$^{-/-}$ = 25.3% ± 1.20, *Stx6*$^{+/-}$
248 = 28.1% ± 0.972, *Stx6*$^{+/+}$ = 24.8% ± 1.26; RML: *Stx6*$^{-/-}$ = 23.7% ± 1.03, *Stx6*$^{+/-}$ = 29.9% ± 1.06,
249 *Stx6*$^{+/+}$ = 24.5% ± 0.899) compared to ~8% in control animals (PBS: *Stx6*$^{-/-}$ = 7.37% ± 1.33,
250 *Stx6*$^{+/-}$ = 8.77% ± 0.525, *Stx6*$^{+/+}$ = 7.09% ± 0.700) (**Fig 6B, D**). Interestingly in all conditions
251 *Stx6*$^{+/-}$ mice demonstrated a modestly higher proportion of microglia relative to both *Stx6*$^{+/+}$
252 and *Stx6*$^{-/-}$ mice, which was significant in RML inoculated animals after adjusting for different
253 ages at death ($P_{adj} = 4.07 \times 10^{-3}$ and $P_{adj} = 1.74 \times 10^{-4}$ respectively).

254

255 ## Discussion

256 Incubation period differences in mice with genetic reduction of syntaxin-6 following
257 intracerebral inoculation with RML and ME7 mouse-adapted scrapie prions.

258 Mouse models are a suitable way to assess the role of human risk genes as they are naturally
259 susceptible to prion diseases, and prion-infected animals faithfully recapitulate many of the
260 key aspects of human disease. In this study, C57BL/6N female mice with genetic reduction of
261 syntaxin-6 showed prolonged mouse prion disease incubation periods for both prion strains
262 tested. However, the observed extension of 12 days in prion-infected *Stx6*$^{-/-}$ animals was
263 modest, which may reflect the moderate effect sizes for typical risk alleles detected by GWAS
264 (*STX6* odds ratio (OR) = 1.16)(3) or potential compensatory mechanisms associated with
265 constitutive gene knockout. Alternatively, it remains possible that modest changes in
266 incubation periods might have resulted from imbalance in unmeasured confounding factors
267 with genotypes being inoculated on different days, or simply chance effects. Indeed, when
268 groups of genetically identical FVB/N were inoculated in different groups at different times,
269 median incubation between individual groups ranged between 103 and 137 days despite
270 intragroup variation being very low(26), substantially greater variation than what was
271 observed between different arms of this study. The modest differences in incubation time
272 observed therefore need cautious interpretation.

273 Although PrP^C levels were comparable between the genotypes suggesting a direct interaction
274 of *Stx6* on *Prnp* expression was not the driving force behind the observation, we cannot
275 exclude subtle effects on the expression or distribution of PrP^C and it remains possible, even
276 likely, that *Stx6* modifying effects are exerted through altered trafficking of PrP^C or disease-

277 associated forms of the protein. Furthermore, considering the syntaxin-6 risk effect was
278 identified for sCJD, such an effect may not be sufficient to substantially modulate incubation
279 times in a prion-infection paradigm using 1% infected brain homogenate with the high
280 infectious prion dose administered being substantially different from a disease-initiating
281 event in sporadic disease. Therefore, future experiments using lower titres are warranted to
282 explore this further.

283 Although we recently identified risk variants associated with sCJD at the *STX6* locus, proximity
284 of risk SNPs to genes is suggestive but not sufficient to establish causality. Integration of
285 GWAS variants with eQTL data provided evidence *STX6* expression is associated with human
286 disease risk. This *in vivo* data is therefore in keeping with the hypothesis derived from GWAS
287 discovery that increased *STX6* expression promotes prion disease pathogenesis. Importantly
288 however, prion transmission studies model a form of acquired prion disease, raising the
289 possibility that syntaxin-6 plays a role across different aetiologies of prion disease and across
290 species.

291 Assessment of prion-related phenotypes

292 No differences in neuronal loss and the extent or distribution of PrP pathology were noted
293 between *Stx6*$^{+/+}$, *Stx6*$^{+/-}$ and *Stx6*$^{-/-}$ mice. This indicates that *Stx6* expression does not alter
294 disease progression through a gross effect on disease pathology. However, it should be noted
295 that this was assessed in endpoint animals where neuropathology was severe and
296 quantification of these was not possible due to processing artefacts, which may have masked
297 more subtle differences. Furthermore, ages of mice were not matched, as *Stx6*$^{-/-}$ mice
298 generally survived longer before culling than the wild-type controls.

299 In contrast, quantitative comparisons of gliosis between the genotypes revealed some subtle
300 differences. Interestingly a ~10% increase in astrocyte count was seen in ME7-infected *Stx6*$^{-/-}$
301 mice and a ~5% increase in microglia count was seen in RML-infected *Stx6*$^{+/-}$ mice relative to
302 *Stx6*$^{+/+}$ animals. Furthermore, in all conditions *Stx6*$^{+/-}$ mice demonstrated a modestly higher
303 proportion of microglia relative to both *Stx6*$^{+/+}$ and *Stx6*$^{-/-}$ mice, which may reflect a dose-
304 dependent effect of *Stx6* expression on microglia function. To exclude the possibility that
305 these differences were driven by different ages of animals at endpoint, we included age at
306 death in days as a covariate in the regression analysis with no significant effect found. Future
307 dissection of time points across the prion incubation period may reveal additional differences
308 in neuropathology or other readouts of disease progression.

309 Considering syntaxin-6 itself has been proposed as a particularly promiscuous SNARE protein
310 with a multitude of cell-type specific functions, it is certainly plausible that the pathological
311 role of syntaxin-6 is mediated through non-neuronal cell types. Taken together, these results
312 suggest a possible role for syntaxin-6 in the supporting cells of the brain, fitting with the
313 increasing acceptance that prion disease pathobiology is driven by the interaction of multiple
314 cell types and non-cell autonomous mechanisms(27, 28).

315 Targeting syntaxin-6 as a therapeutic strategy

316 Human genetic evidence increasingly supports successful drug development
317 programmes(29). The identification and proposal of *STX6* as a risk gene through GWAS
318 therefore provokes research about therapeutic potential, which is in part supported by this
319 *in vivo* study. Importantly for therapeutic utility, *Stx6*$^{-/-}$ mice are viable and fertile with no
320 gross neurological or physiological impairments. Although the IMPC have recorded some
321 potential metabolic and behavioural alterations in *Stx6*$^{-/-}$ mice, these were not reproducible

322 across life stages and gender, and were not replicated in our mouse cohort. However, the
323 very modest extension in incubation period with full knockout of syntaxin-6 does raise the
324 question of whether partial reduction in syntaxin-6 levels in established disease would result
325 in a meaningful clinical benefit. Further work involves determining the efficacy of targeting
326 *Stx6* during the disease course. Furthermore, the pleiotropic role of syntaxin-6 across multiple
327 neurodegenerative diseases, including PSP and AD, raises the potential that *STX6*-targeting
328 therapies could have wider applicability to other neurodegenerative diseases, warranting
329 further investigation.

330 Potential mechanistic roles of syntaxin-6 in prion disease pathology

331 As a key intracellular trafficking protein, it is plausible that modified syntaxin-6 function alters
332 the transport of PrP^C and/or disease-associated prions throughout the cell and several
333 possible mechanisms are plausible. Considering syntaxin-6 is thought to be involved in the
334 recycling of proteins from endosomes(30, 31), knockout of *Stx6* could conceivably result in
335 reduced transport of disease-associated PrP away from these structures and thus increased
336 degradation in the lysosomal pathway, with obvious benefits for prion load. Alternatively a
337 similar hypothesis could be proposed for transport of toxic species in prion diseases. Recent
338 work indicated a role of syntaxin-6 in the kinetic formation of toxic PrP structures *in vitro*,
339 however whether a direct protein interaction occurs *in vivo* is unclear(32). Finally, it is
340 plausible the effect of modified syntaxin-6 function has more widespread implications for
341 cellular function, which may indirectly affect prion disease biology.

342

343 ## Materials and Methods

344 *Ethical approval*

345 Work was performed under approval and license granted by the UK Home Office (Animals
346 (Scientific Procedures) Act 1986), which conformed to UCL institutional and Animal Research:
347 Reporting of In Vivo Experiments (ARRIVE) guidelines. Experiments were approved by the
348 MRC Prion Unit Animal Research Scientific Committee.

349 *Mice*

350 *Stx6*$^{+/-}$ mice (C57BL/6NTac-*Stx6*$^{em1(IMPC)H}$/H) were generated at MRC Harwell and crossbred to
351 establish homozygous *Stx6*$^{-/-}$ and *Stx6*$^{+/+}$ lines, which were used to populate the experimental
352 cohorts. *Stx6*$^{+/-}$ litters were obtained through crossbreeding of these two lines.

353 *Genotyping*

354 DNA was extracted from standard ear biopsies. The presence of a 108 bp deletion in *Stx6* was
355 determined using two PCR reactions with the following primer combinations with GoTaq G2
356 Hot Start Polymerase (Promega): PCR 1 forward 5'- CGATCTGTGAGACTCATCGGG and reverse
357 5'-GGGAGTCCTAACACCACCTTC, PCR 2 forward 5'-CCTGACTCTCTGATAGCCAC and reverse 5'-
358 ACAAAACCAAAGCCTGCAC. PCR reactions were analysed by agarose gel electrophoresis and
359 image capture was performed on a Universal Hood II Gel Doc System (Bio-Rad).

360 *Western blot of mouse brain homogenate for syntaxin-6*

361 Brains from mice at 61-65 days were dissected on the sagittal plane and flash frozen.
362 Following weighing, samples were ribolysed in Dulbecco's phosphate-buffered saline (DPBS)

363 with ceramic homogenisation beads (Bertin Technologies) at max speed for 105 sec to
364 produce 10 and 20% homogenates were stored at -80° C until use.

365 Homogenates were diluted in DPBS with 4X SDS sample buffer (250 mM Tris base, 40%
366 glycerol, 8% SDS, 0.04% bromophenol blue) and boiled at 95°C for 5 min. 35 µg of total protein
367 was loaded onto a 4-12% (w/v) Bis-Tris polyacrylamide gel (Invitrogen) and electrophoresed
368 before being electroblotted to a nitrocellulose membrane. Membranes were blocked in
369 Odyssey Blocking Buffer for 1 h at room temperature (RT), before incubation with anti-
370 syntaxin-6 (1:500 clone C34B2 (Cell Signalling; 2869S) or clone 3D10 (Abcam; Ab12370))
371 overnight at 4°C. Membranes were washed with 0.05% Tween-20 in phosphate buffered
372 saline (PBST) for 3 x 5 min with agitation and incubated with anti-β actin (1:1000 rabbit
373 polyclonal (Sigma Aldrich; A2066) or 1:5000 mouse monoclonal (Sigma Aldrich; A5441)). After
374 washing, membranes were probed with fluorophore-conjugated secondary antibodies (IRDye
375 800CW Donkey anti-rabbit IgG and IRDye 680RD goat anti-mouse IgG both at1:4000) for 1 h
376 at RT. Membranes were washed again and imaged with Odyssey Gel Documentation System
377 (LI-COR; Model 9120).

378 *ELISA for PrP^C expression*

379 Brain homogenates were initially diluted to 3.5 mg/ml total protein in PBS to a final volume
380 of 40 µl. 5 µM AEBSF and 2.5% w/v SDS was added to each sample and boiled at 100°C for 10
381 min. Samples were aliquoted and stored at -80°C until use.

382 A high-binding 96-well flat bottom plate was pre-coated with 100 µl of 2.5 µg/ml anti-PrP
383 ICSM18 antibody in 0.05 M carbonate coating buffer (0.035 M $NaHCO_3$, 0.015 M Na_2CO_3, pH
384 9.6) and incubated at 4°C overnight before washing x3 with 1% PBST.

385 240 µl pre-heated capture buffer (37°C, 30X, pH 8.4; 2% N-Lauroylsarcosyl, 2% BSA, 2% Triton
386 X-100, 50 mM Tris base pH 8.0) was added to 8 µl sample and 50 µl added to wells in triplicate.
387 Plates were incubated at 37°C for 1 h before washing x3 with 1% PBST. For detection of bound
388 PrP, 100 µl of 1 µg/ml biotinylated anti-PrP ICSM35 antibody diluted in 1% PBST was added
389 to each well, incubated at 37°C for 15 min and washed as previous. 100 µl streptavidin-HRP
390 diluted 1:10,000 in PBST was then added and incubated at 37°C for 15 min, prior to
391 development with QuantaBlu Fluorogenic Peroxidase Substrate Kitas per manufacturer's
392 instructions (Thermo Scientific). Plates were imaged using Tecan Infinite M200 plate reader
393 with 313 nm and 398 nm excitation and emission wavelengths respectively.

394 *Inoculation study*

395 Anaesthetised female *Stx6*$^{-/-}$, *Stx6*$^{+/-}$ and *Stx6*$^{+/+}$ mice were inoculated intracerebrally in the
396 right parietal lobe with 30 µl 1% (w/v) C57BL/6 mouse-adapted RML or ME7 prion-infected
397 brain homogenate at 6-8 weeks of age (n = 20/group), as previously described(33), or with
398 PBS (n = 5/group). Experimental arms were inoculated on different days. Each individual
399 mouse was considered an experimental unit. Group sizes of 20 mice per experimental
400 condition were used to provide sufficient power to detect a 5% difference in incubation
401 periods, calculated assuming an approximate minimum incubation period of 150 days with a
402 standard deviation of 7.5 days estimated from previously published studies with C57BL/6
403 mice(17, 34), whilst allowing for loss due to incurrent illness (as expected from previous
404 experiments of similar length (unpublished data)). Animals were allocated to groups based on
405 genotypes. The animal technicians tasked with diagnosing scrapie sickness were blind to study
406 design.

407 Mice were monitored daily and culled following diagnosis with scrapie sickness according to
408 established criteria or identification of distinct health concerns(33). Incubation period was
409 defined as the number of days from inoculation until definite scrapie diagnosis(33), with
410 animals censored when culled due to other reasons (health concerns/adverse events outlined
411 *a priori* in the Project licence) or found dead (**Error! Reference source not found.**).

412 Disease-free incubation period was defined as the number of days from inoculation to onset
413 of the first scrapie-associated neurological symptom, with animals censored in the previous
414 analysis due to wet genital region included in this analysis as a previously reported symptom
415 of scrapie sickness (data unpublished). Mice culled due to other health concerns not known
416 to be related to prion disease remained censored from this analysis (**Error! Reference source**
417 **not found.**). Animals culled prior to onset of any neurological symptoms were excluded due
418 to missingness.

419 Kaplan-Meier survival curves and analyses were generated using RStudio packages "survival"
420 and "survminer" and survival differences analysed using a log-rank test.

421 *Western blot for prion strain typing*

422 Following culling, brains were removed, dissected on the sagittal plane with one hemisphere
423 flash frozen and stored at -80ºC until brain homogenate preparation. 20% (w/v) homogenates
424 were prepared in DPBS by ribolysing with ceramic homogenisation beads (Fisherbrand
425 Zirconium Ceramic Oxide Bulk Beads) at 6,500 rpm for 45 sec using the Hybaid Riboylser. 20%
426 homogenates were stored at -80°C until use. 20 µL aliquots of 10% (w/v) brain homogenates
427 were prepared in DPBS. 1 µL benzonase was added and left to incubate for 10 min at RT

428 followed by 1 h incubation with proteinase K (PK; 50 µg/mL or 100 µg/mL final concentration
429 for ME7 and RML respectively) at 37°C with agitation (800 rpm).

430 Samples were mixed with 2X Lithium Dodecyl Sulphate Sample Buffer (2x dilution NuPAGE™
431 LDS Sample Buffer (4X) and 5x dilution NuPAGE™ Sample Reducing Agent (10X)) with 4-(2-
432 Aminoethyl) benzenesulfonyl fluoride hydrochloride (AEBSF) (4 mM final concentration).
433 Samples were immediately transferred to a 100 °C heating block for 10 min. Following a 1 min
434 spin at 21,000 x g, electrophoresis was performed on 12% (w/v) bis-tris gels (Invitrogen) with
435 SeeBlue Prestained Molecular Weight Marker prior to electroblotting to Immobilon PVDF
436 membrane (Millipore).

437 Membranes were blocked in PBST with 5% (w/v) non-fat dried skimmed milk powder and
438 then probed with ICSM35 anti-PrP antibody (D-Gen Ltd; 1:5000 for RML) or with 6D11 anti-
439 PrP antibody (BioLegend (808004); 1:5000 for ME7) in PBST overnight. After washing (3 x 5
440 min followed by 3 x 15 min) the membranes were probed with a 1:10,000 dilution of alkaline-
441 phosphatase-conjugated goat anti-mouse IgG secondary antibody (Sigma-Aldrich (A2179)) in
442 PBST. After washing (1 h with PBST as before and 2 × 5 min with 20 mM Tris pH 9.8 containing
443 1 mM $MgCl_2$) blots were incubated for 5 min in chemiluminescent substrate (CDP-Star; Tropix
444 Inc) and visualized on Biomax MR film (Kodak).

445 *Immunohistochemistry of prion-related neuropathology*

446 Immunohistochemistry was performed as previously described with modifications(35). Half
447 mouse brains were fixed in 10% buffered formal-saline, processed, paraffin wax embedded
448 and serial sections of 5 µm nominal thickness were taken. Deparaffinised sections were
449 investigated for abnormal PrP, microgliosis and astrocytosis on the Ventana Discovery XT

450 automated IHC staining machine (Roche Tissue Diagnostics) as described in(36). In the PBS
451 inoculated controls, 4 x *Stx6*$^{-/-}$, 5 x *Stx6*$^{+/-}$ and 5 x *Stx6*$^{+/+}$ animals were analysed (due to one
452 *Stx6*$^{-/-}$ mouse lost due to incurrent illness). In the RML inoculated groups, 10 mice were
453 analysed for each genotype. In the ME7 inoculated groups, 10 mice were analysed for *Stx6*$^{+/+}$
454 and *Stx6*$^{+/-}$ groups and 7 mice in the *Stx6*$^{-/-}$ group (only mice culled due to scrapie sickness
455 analysed for histology). All 20 mice were analysed for neuronal loss in each group.

456 Anti-PrP monoclonal antibody ICSM35 (D-Gen Ltd) was used with biotinylated polyclonal
457 rabbit anti-mouse immunoglobulin secondary antibodies (Dako; Agilent) and Ventana
458 proprietary detection reagents utilizing 3,3'-diaminobenzidine tetrahydrochloride as the
459 chromogen (DAB Map Detection Kit; Roche Tissue Diagnostics). Sections were treated with
460 Discovery CC1 cell conditioning solution at 95°C for 60 min followed by a low concentration
461 of protease (Protease 3) for 12 min prior to staining.

462 Anti-iba1 microglial antibody (AlphaLaboratories) or anti-GFAP antibody (Agilent) were used
463 with biotinylated polyclonal goat anti-rabbit immunoglobulin secondary antibodies (Dako;
464 Agilent) and Ventana proprietary detection reagents (DAB Map Detection Kit). Sections were
465 treated with Discovery CC1 cell conditioning solution at 95°C for 60 min or a medium
466 concentration of protease (Protease 1) for 4 min respectively prior to staining.

467 Conventional methods on a Gemini AS Automated Slide Stainer were used for haematoxylin
468 staining. Positive staining controls for the staining technique were used throughout. Slides
469 were digitally scanned on Hamamatsu NanoZoomer 360, images captured from the
470 NDP.serve3 (NanoZoomer Digital Pathology) or NZConnect software and composed with
471 Adobe Photoshop.

472 *Immunohistochemistry quantification and statistical analysis*

473 GFAP and Iba1 immunostaining in whole brain sections was quantified using QuPath (v0.3.0)
474 software (4-5 PBS-inoculated mice; 7-10 prion-inoculated mice). Colour deconvolution was
475 performed to distinguish DAB staining from haematoxylin background and pixel classification
476 used to select tissue for analysis (whole brain). Pixel classification selected regions positive
477 for DAB staining (classifier trained on 10% total images). Area positive for DAB staining was
478 calculated for each image and % area stained calculated relative to total tissue area analysed.
479 Statistical differences were determined using a linear regression model with age at death
480 included as a confounding variable in RStudio (v1.1.463) software.

481 *Immunohistochemistry of peripheral organs*

482 The following organs were harvested from PBS-inoculated wildtype *Stx6*$^{+/+}$, *Stx6*$^{+/-}$ and *Stx6*$^{-/-}$
483 female mice at 56-61 weeks of age: liver, pancreas, kidney, skeletal muscle and adipose tissue.
484 Organs were fixed in 10% buffered formal-saline and processed for haematoxylin staining as
485 previously described. Tissues were visually assessed for expected architecture integrity and
486 for vacuolation in a semi-quantitative manner.

487 *Computer Tomography (CT) scanning*

488 *Stx6*$^{+/+}$ (n = 2) and *Stx6*$^{-/-}$ (n = 2) male mice were culled at 12 weeks of age and frozen at -20 °C
489 until CT scanning. Bone abnormalities were assessed using the Quantum x2 microCT scanner.
490 Analysis was done on Analyse 14.0 software.

491 *Clinical chemistry analysis*

492 Terminal blood was collected from 100 day old *Stx6*$^{+/+}$ and *Stx6*$^{-/-}$ animals by post-mortem
493 cardiac puncture. Serum was prepared by allowing clotting for 10 mins followed by
494 centrifugation at 2600 g at 4°C for 12 minutes. Serum was stored in polypropylene tubes at -
495 80°C prior to assessment of blood metabolites using the AU680 Analyser.

496

Acknowledgments

We thank Florin Pintilii, Helena Costa and Fabio Argentina for further technical assistance with immunohistochemistry, Dr Jonathan Wadsworth for training support and preparation of the inoculum, the staff of the MRC Prion Unit at UCL Biological Services Facility for animal husbandry and care, Nick Kaye and Craig Fitzhugh for experimental assistance, Dr Tammy Kalber for assistance with CT scanning and Shyma Hamdan for assistance with animal genotyping. This work was funded by the UK Medical Research Council. Simon Mead and John Collinge are National Institute for Health Research Senior Investigators.

Data availability

All data is available in **Supplementary Tables**.

References

1. Kraus A, Hoyt F, Schwartz CL, Hansen B, Artikis E, Hughson AG, et al. High-resolution structure and strain comparison of infectious mammalian prions. Mol Cell. 2021;81(21):4540-51 e6.
2. Manka SW, Zhang W, Wenborn A, Betts J, Joiner S, Saibil HR, et al. 2.7 Å cryo-EM structure of ex vivo RML prion fibrils. Nature Communications. 2022;13(1):4004.
3. Jones E, Hummerich H, Viré E, Uphill J, Dimitriadis A, Speedy H, et al. Identification of novel risk loci and causal insights for sporadic Creutzfeldt-Jakob disease: a genome-wide association study. The Lancet Neurology. 2020;19(10):840-8.
4. Höglinger GU, Melhem NM, Dickson DW, Sleiman PMA, Wang L-S, Klei L, et al. Identification of common variants influencing risk of the tauopathy progressive supranuclear palsy. Nature Genetics. 2011;43(7):699-705.
5. Ferrari R, Ryten M, Simone R, Trabzuni D, Nicolaou N, Hondhamuni G, et al. Assessment of common variability and expression quantitative trait loci for genome-wide associations for progressive supranuclear palsy. Neurobiology of Aging. 2014;35(6):1514.e1-.e1.
6. Wingo AP, Liu Y, Gerasimov ES, Gockley J, Logsdon BA, Duong DM, et al. Integrating human brain proteomes with genome-wide association data implicates new proteins in Alzheimer's disease pathogenesis. Nature Genetics. 2021;53(2):143-6.
7. Yu L, Boyle PA, Wingo AP, Yang J, Wang T, Buchman AS, et al. Neuropathologic Correlates of Human Cortical Proteins in Alzheimer Disease and Related Dementias. Neurology. 2021.
8. Bock JB, Lin RC, Scheller RH. A new syntaxin family member implicated in targeting of intracellular transport vesicles. The Journal of biological chemistry. 1996;271(30):17961-5.
9. Bock JB, Klumperman J, Davanger S, Scheller RH. Syntaxin 6 functions in trans-Golgi network vesicle trafficking. Molecular biology of the cell. 1997;8(7):1261-71.
10. Zerr I, Kallenberg K, Summers DM, Romero C, Taratuto A, Heinemann U, et al. Updated clinical diagnostic criteria for sporadic Creutzfeldt-Jakob disease. Brain. 2009;132(Pt 10):2659-68.
11. Chandler RL. Encephalopathy in mice produced by inoculation with scrapie brain material. Lancet. 1961;1(7191):1378-9.
12. Aguzzi A, Barres BA, Bennett ML. Microglia: scapegoat, saboteur, or something else? Science (New York, NY). 2013;339(6116):156-61.
13. Fraser H, Dickinson AG. Scrapie in mice. Agent-strain differences in the distribution and intensity of grey matter vacuolation. J Comp Pathol. 1973;83(1):29-40.
14. Zlotnik I, Rennie JC. Further observations on the experimental transmission of scrapie from sheep and goats to laboratory mice. J Comp Pathol. 1963;73:150-62.
15. Sandberg MK, Al-Doujaily H, Sharps B, Clarke AR, Collinge J. Prion propagation and toxicity in vivo occur in two distinct mechanistic phases. Nature. 2011;470(7335):540-2.
16. Sandberg MK, Al-Doujaily H, Sharps B, De Oliveira MW, Schmidt C, Richard-Londt A, et al. Prion neuropathology follows the accumulation of alternate prion protein isoforms after infective titre has peaked. Nature Communications. 2014;5(1):4347.
17. Akhtar S, Grizenkova J, Wenborn A, Hummerich H, Fernandez de Marco M, Brandner S, et al. Sod1 deficiency reduces incubation time in mouse models of prion disease. PloS one. 2013;8(1):e54454.
18. Grizenkova J, Akhtar S, Hummerich H, Tomlinson A, Asante EA, Wenborn A, et al. Overexpression of the Hspa13 (Stch) gene reduces prion disease incubation time in mice. Proceedings of the National Academy of Sciences of the United States of America. 2012;109(34):13722-7.
19. Groza T, Gomez FL, Mashhadi HH, Muñoz-Fuentes V, Gunes O, Wilson R, et al. The International Mouse Phenotyping Consortium: comprehensive knockout phenotyping underpinning the study of human disease. Nucleic Acids Research. 2022:gkac972.

20. Büeler H, Aguzzi A, Sailer A, Greiner RA, Autenried P, Aguet M, et al. Mice devoid of PrP are resistant to scrapie. Cell. 1993;73(7):1339-47.
21. Dickinson ME, Flenniken AM, Ji X, Teboul L, Wong MD, White JK, et al. High-throughput discovery of novel developmental phenotypes. Nature. 2016;537(7621):508-14.
22. Carlson GA, Kingsbury DT, Goodman PA, Coleman S, Marshall ST, DeArmond S, et al. Linkage of prion protein and scrapie incubation time genes. Cell. 1986;46(4):503-11.
23. Budka H. Neuropathology of prion diseases. British Medical Bulletin. 2003;66(1):121-30.
24. Wenborn A, Terry C, Gros N, Joiner S, D'Castro L, Panico S, et al. A novel and rapid method for obtaining high titre intact prion strains from mammalian brain. Scientific Reports. 2015;5(1):10062.
25. Makarava N, Chang JC, Kushwaha R, Baskakov IV. Region-Specific Response of Astrocytes to Prion Infection. Front Neurosci. 2019;13:1048.
26. Tamgüney G, Giles K, Glidden DV, Lessard P, Wille H, Tremblay P, et al. Genes contributing to prion pathogenesis. The Journal of general virology. 2008;89(Pt 7):1777-88.
27. Tahir W, Abdulrahman B, Abdelaziz DH, Thapa S, Walia R, Schätzl HM. An astrocyte cell line that differentially propagates murine prions. The Journal of biological chemistry. 2020;295(33):11572-83.
28. Smith HL, Freeman OJ, Butcher AJ, Holmqvist S, Humoud I, Schätzl T, et al. Astrocyte Unfolded Protein Response Induces a Specific Reactivity State that Causes Non-Cell-Autonomous Neuronal Degeneration. Neuron. 2020;105(5):855-66.e5.
29. Ochoa D, Karim M, Ghoussaini M, Hulcoop DG, McDonagh EM, Dunham I. Human genetics evidence supports two-thirds of the 2021 FDA-approved drugs. Nat Rev Drug Discov. 2022.
30. Mallard F, Tang BL, Galli T, Tenza D, Saint-Pol A, Yue X, et al. Early/recycling endosomes-to-TGN transport involves two SNARE complexes and a Rab6 isoform. J Cell Biol. 2002;156(4):653-64.
31. Chao DS, Hay JC, Winnick S, Prekeris R, Klumperman J, Scheller RH. SNARE membrane trafficking dynamics in vivo. J Cell Biol. 1999;144(5):869-81.
32. Sangar D, Jack K, Batchelor M, Mistry B, Bieschke J. Syntaxin 6 delays prion protein fibril formation and prolongs presence of toxic aggregation intermediates. bioRxiv. 2022:2022.08.25.505283.
33. O'Shea M, Maytham EG, Linehan JM, Brandner S, Collinge J, Lloyd SE. Investigation of Mcp1 as a Quantitative Trait Gene for Prion Disease Incubation Time in Mouse. Genetics. 2008;180(1):559-66.
34. Akhtar S, Wenborn A, Brandner S, Collinge J, Lloyd SE. Sex Effects in Mouse Prion Disease Incubation Time. PloS one. 2011;6(12):e28741.
35. Wadsworth JDF, Joiner S, Linehan JM, Jack K, Al-Doujaily H, Costa H, et al. Humanised transgenic mice are resistant to chronic wasting disease prions from Norwegian reindeer and moose. J Infect Dis. 2021.
36. Wadsworth JDF, Adamson G, Joiner S, Brock L, Powell C, Linehan JM, et al. Methods for Molecular Diagnosis of Human Prion Disease. Methods Mol Biol. 2017;1658:311-46.

597 ## Figures

598 ***Fig 1: Development and validation of Stx6 knockout mice. (A)*** *Strategy for CRISPR/Cas9-*
599 *mediated knockout of Stx6 in C57BL/6N mice. Four single guide RNAs (sgRNAs) targeting the*
600 *DNA sequences in exons 5 and 6 of the two main Stx6 protein-coding transcripts (Stx6-201 and*
601 *Stx6-209), also encompassing the N-terminal portion of the shorter Stx6-206 transcript, were*
602 *selected for gene editing in zygotes. This resulted in an 1808 nucleotide (nt) deletion replaced*
603 *by an 8 nt insertion. Top: Full Stx6 gene in the genome. Bottom: protein coding transcripts.*
604 *Inset: CRISPR/Cas9 genome editing at Stx6 locus.* ***(B)*** *Representative quantitative*
605 *immunoblots with anti-syntaxin 6 and anti-β actin antibodies of whole brain homogenates*
606 *from $Stx6^{+/-}$, $Stx6^{-/-}$ and $Stx6^{+/+}$ mice and* ***(C)*** *quantification of syntaxin-6 intensity relative to*
607 *β-actin normalised to $Stx6^{+/+}$ control demonstrates loss of primary ~32 kDa protein isoform in*
608 *$Stx6^{-/-}$ mice (0.0757% ± 0.0217 (mean ± SEM)) with ~50% expression (55.9% ± 0.0436) in $Stx6^{+/-}$*
609 *mice (n = 3 per group, n = 3 technical replicates).* ***(D)*** *Analysis of PrP^{C} expression in whole brain*
610 *homogenates from $Stx6^{-/-}$, $Stx6^{+/-}$ and $Stx6^{+/+}$ early adult 9 week old mice by ELISA does not*
611 *indicate any significant differences between lines ($Stx6^{+/+}$: 6115 ± 838.3 relative fluorescent*
612 *units (RFU); $Stx6^{+/-}$: 5784 ± 1100 RFU; $Stx6^{-/-}$: 5834 ± 153 RFU) (one-way ANOVA on square*
613 *root transformed data).*

614 ***Fig 2: Multi-organ H&E staining shows expected tissue architecture and appearance in $Stx6^{-}$***
615 ***$^{/-}$ and $Stx6^{+/-}$ mice which lack consistent tissue-intrinsic pathologies.*** *The following organs*
616 *were harvested from $Stx6^{+/+}$ (n = 5), $Stx6^{+/-}$ (n = 5) and $Stx6^{-/-}$ (n = 4) female mice at 56-61*
617 *weeks of age: liver, pancreas, kidney, skeletal muscle and white adipose. These were formalin*
618 *fixed, processed to paraffin and underwent H&E staining, revealing no consistent differences*
619 *between genotypes. Scale bar corresponds to 120 µm (a-l), and 500 µm (m-o).*

620 ***Fig 3: Incubation periods in mice with Stx6 reduction following intracerebral inoculation***
621 ***with RML and ME7 mouse-adapted scrapie prions.*** *(**A**-**D**) Kaplan-Meier curve of survival*
622 *probability following intracerebral inoculation of Stx6$^{-/-}$ (red), Stx6$^{+/-}$ (grey) and Stx6$^{+/+}$ (blue)*
623 *C57BL/6N mice (n = 20 per group) with 1% brain homogenate from (**A**,**B**) RML and (**C**,**D**) ME7*
624 *infected C57BL/6N mice. (**A**, **C**) Survival probability until animals were culled due to scrapie*
625 *sickness shows a 12-day increase in median incubation period for (**A**) both Stx6$^{-/-}$ and Stx6$^{+/-}$*
626 *mice following RML inoculation and (**C**) for Stx6$^{-/-}$ mice only following ME7 inoculation relative*
627 *to Stx6$^{+/+}$ mice. (**B**,**D**) Disease-free survival probability (time until onset of the first scrapie*
628 *symptom) (**B**) does not show a significant association with Stx6 genotype following RML-*
629 *inoculation but a nominal 5-day increase in median incubation period in Stx6$^{-/-}$ mice compared*
630 *to (**D**) a 7-day increase in Stx6$^{-/-}$ mice inoculated with ME7, relative to Stx6$^{+/+}$ mice. P-values*
631 *indicate statistical associations with group determined using a log-rank test. Median*
632 *incubation period shown below each plot. Crosses indicate censored animals.*

633 ***Fig 4: Knockout of Stx6 does not alter PrP deposition in prion infected mice.***
634 *Immunohistochemistry using anti-PrP antibody ICSM35 in whole brain (left) with schematic*
635 *depiction of PrP deposition (pink shading: moderate PrP deposition; red shading: intense PrP*
636 *deposition; red dots: PrP micro-plaques) or representative images from striatum, cortex and*
637 *midbrain (middle) from Stx6$^{-/-}$, Stx6$^{+/-}$ and Stx6$^{+/+}$ mice inoculated with PBS (top) or ME7*
638 *(middle) and RML (bottom) mouse-adapted scrapie prions, shows expected PrP deposition in*
639 *all prion-inoculated samples at end-point, with widespread diffuse staining for both strains*
640 *and additional presence of micro-plaques with ME7 (yellow arrows). There was no evidence*
641 *of spontaneous PrP deposition in control animals or gross difference evident between*
642 *genotypes.*

643 ***Fig 5: Neuronal loss and spongiform change were comparable in end-stage Stx6$^{-/-}$, Stx6$^{+/-}$***
644 ***and Stx6$^{+/+}$ mice.*** *Haematoxylin and eosin (H&E) staining of whole brain (left) with schematic*
645 *depiction of spongiosis (right; light purple shading: widely dispersed spongiosis; darker purple*
646 *shading: intense focal spongiosis; yellow shading: neuronal loss) and representative images*
647 *from striatum, cortex and midbrain (middle) from Stx6$^{-/-}$, Stx6$^{+/-}$ and Stx6$^{+/+}$ mice inoculated*
648 *with PBS (top) or ME7 (middle) and RML (bottom) mouse-adapted scrapie prions shows*
649 *expected spongiform pathology in all samples at end-point, including hippocampal neuronal*
650 *loss with ME7, with no gross differences evident between genotypes. No neuropathology was*
651 *evident in PBS-inoculated controls.*

652 ***Fig 6: Variable effect of Stx6 genotype on neuroinflammation in prion disease.*** *(**A**, **B**)*
653 *Example images of immunohistochemistry in Stx6$^{-/-}$, Stx6$^{+/-}$ and Stx6$^{+/+}$ mice inoculated PBS*
654 *control or ME7 and RML mouse-adapted scrapie prions with (**A**) anti-GFAP antibody to*
655 *measure reactive astrocytes and (**B**) anti-Iba1 antibody to measure microgliosis, shows*
656 *expected neuroinflammation in prion-infected animals, including expected intense staining in*
657 *the thalamus with both antibodies and intense GFAP staining in the hippocampus. (**C**, **D**)*
658 *Quantification of percentage area stained with (**C**) anti-GFAP and (**D**) anti-Iba1 antibody*
659 *demonstrates a ~10% increase in astrocyte area in ME7-inoculated Stx6$^{-/-}$ animals and a ~5%*
660 *increase in microglia area in Stx6$^{+/-}$ mice in RML-inoculated animals (linear regression model*
661 *adjusted for age of death; ** $P < 0.01$, *** $P < 0.001$).*

662 **Figure 1**

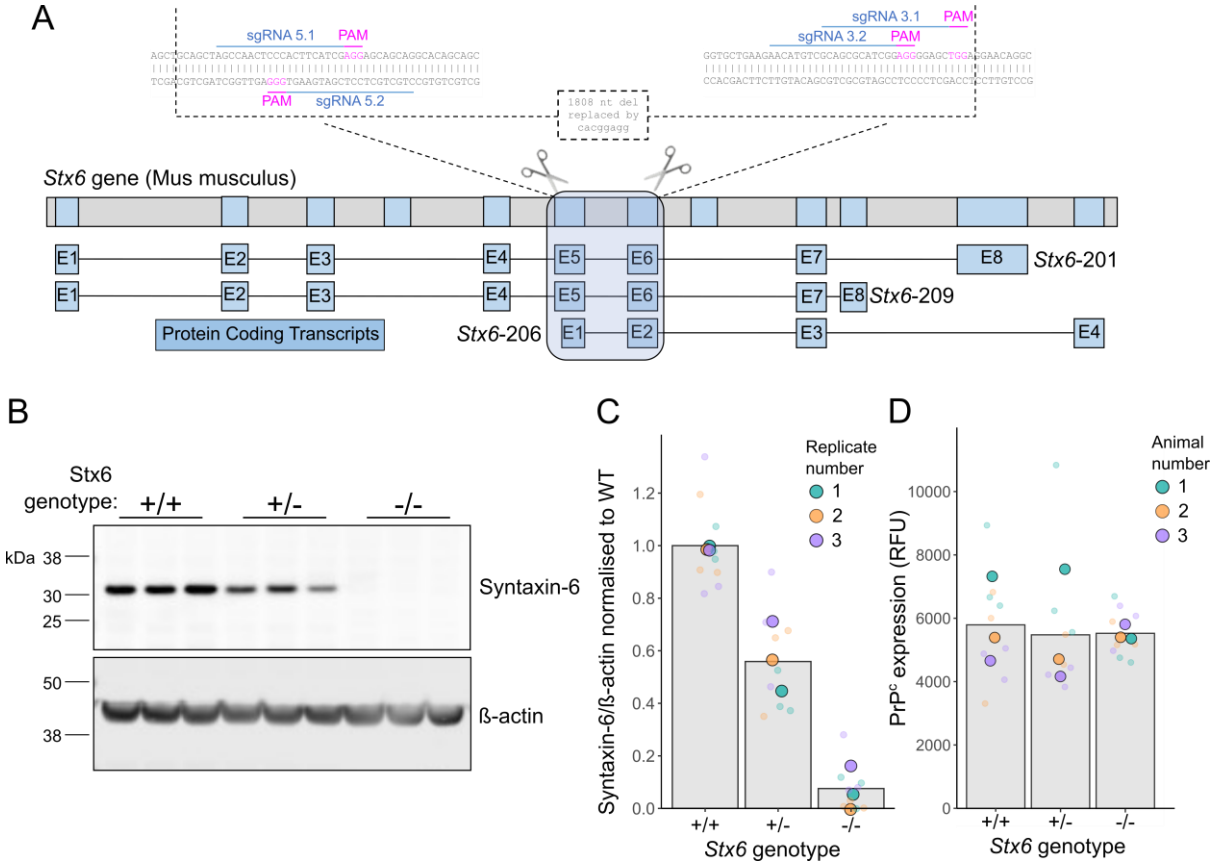

663

664

665 **Figure 2**

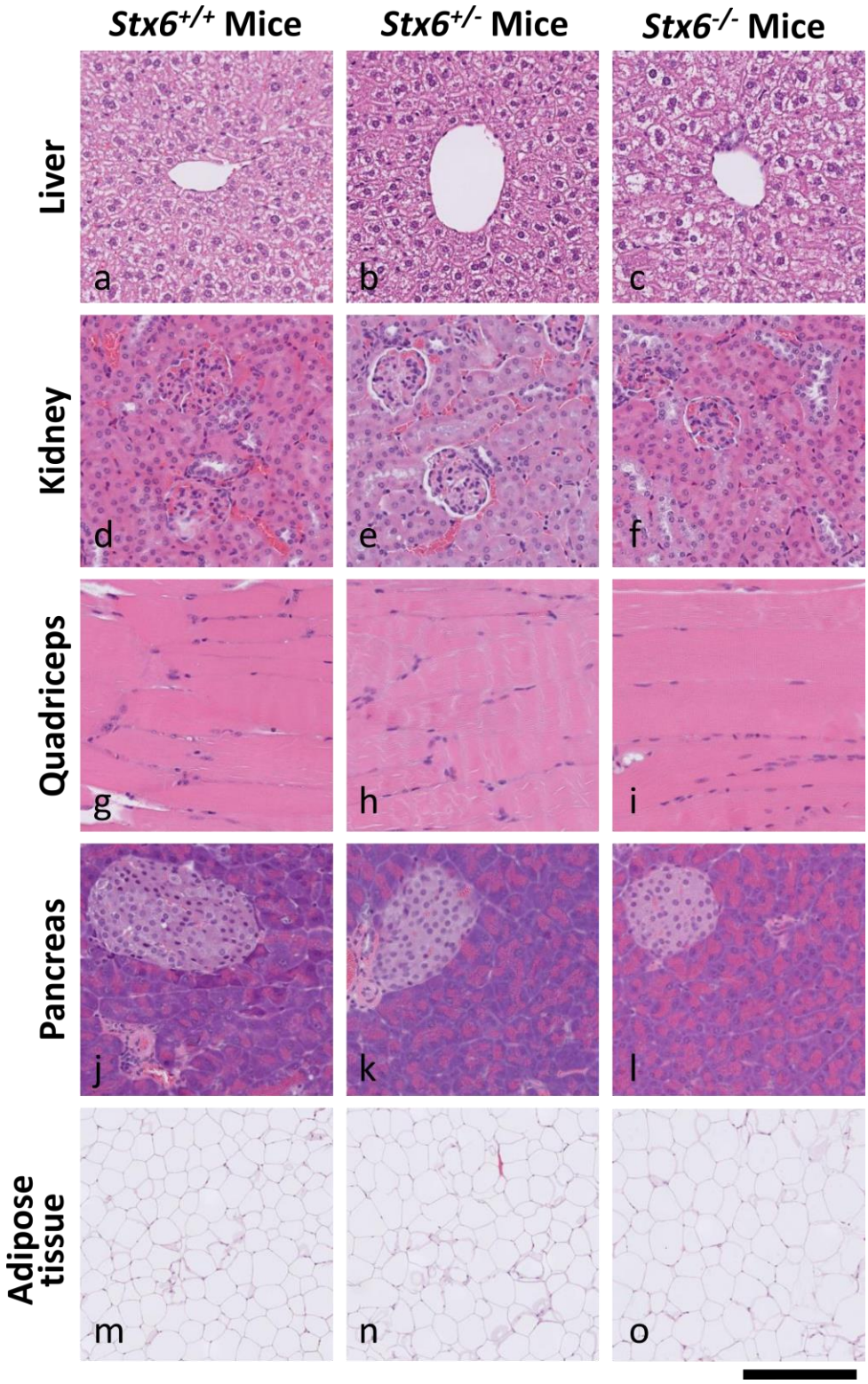

666

667 **Figure 3**

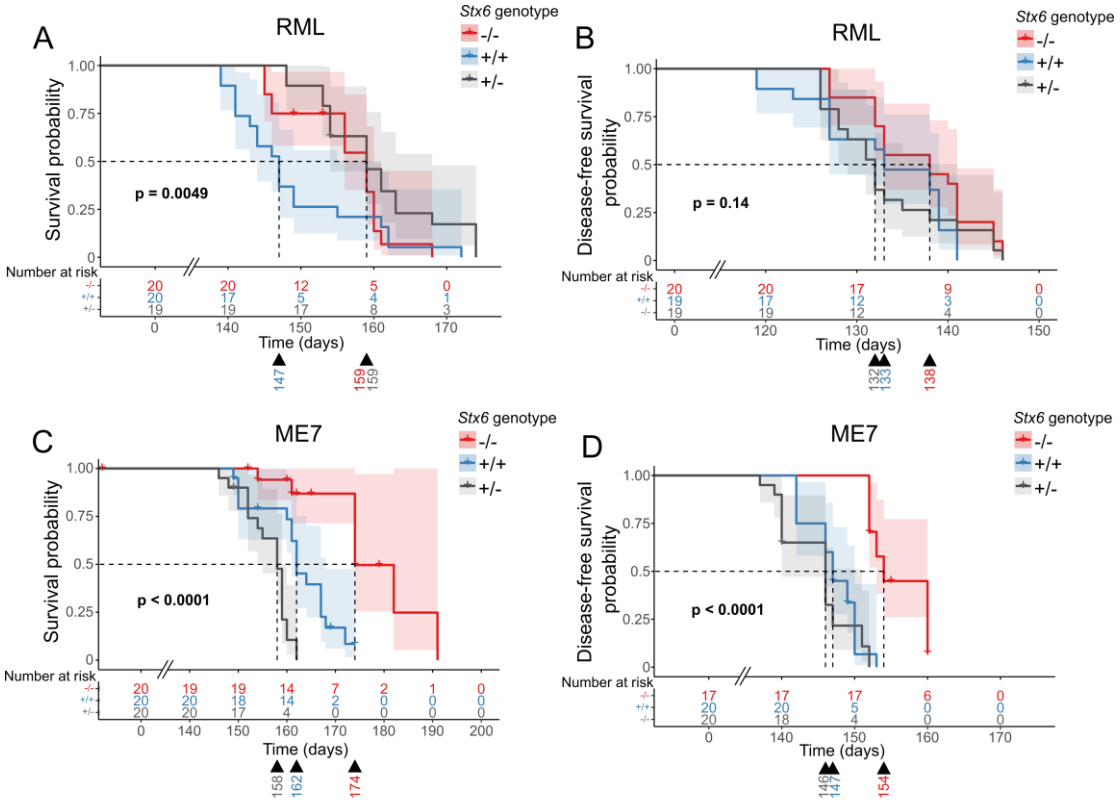

668

669 **Figure 4**

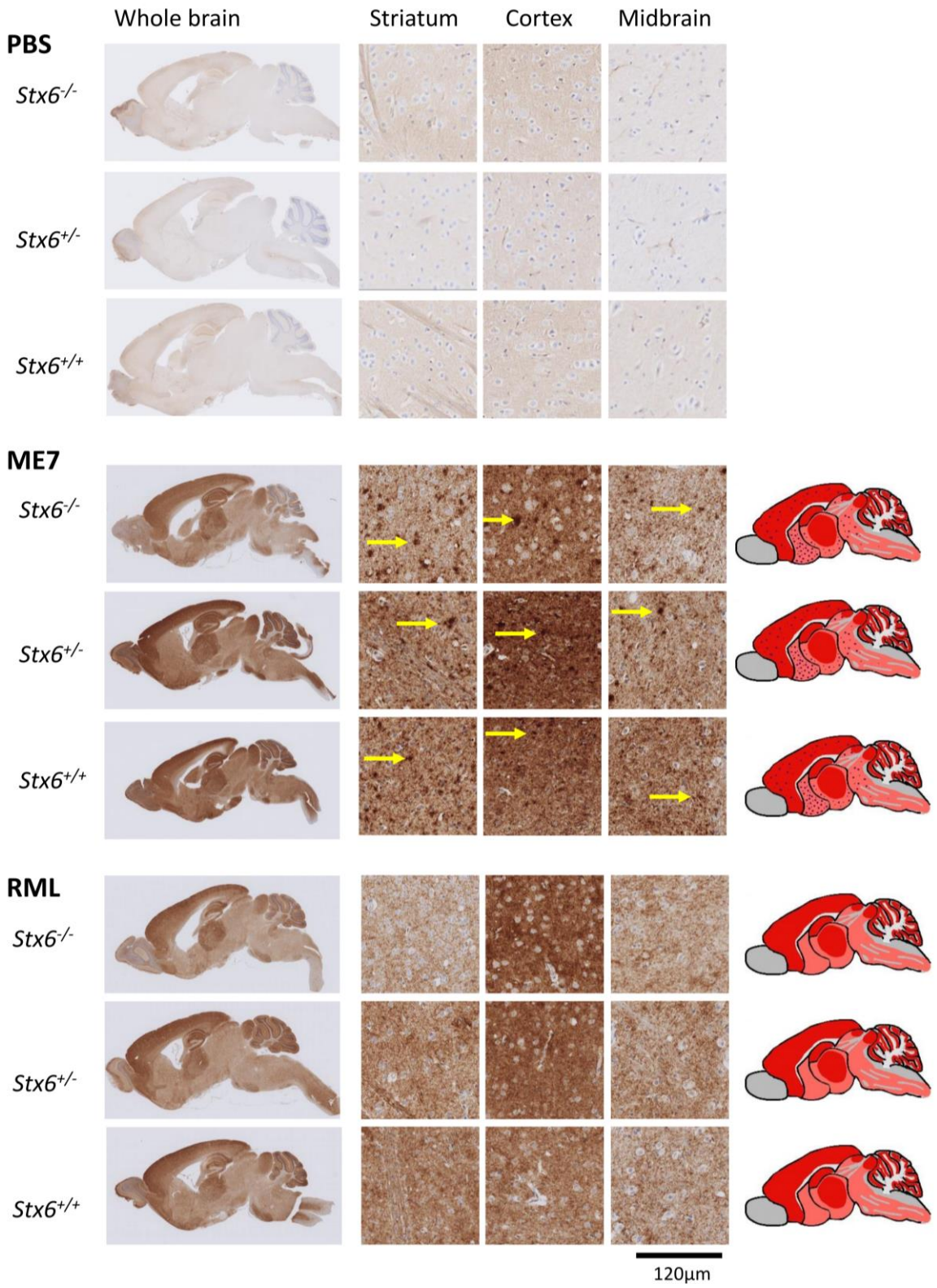

670

671

672 **Figure 5**

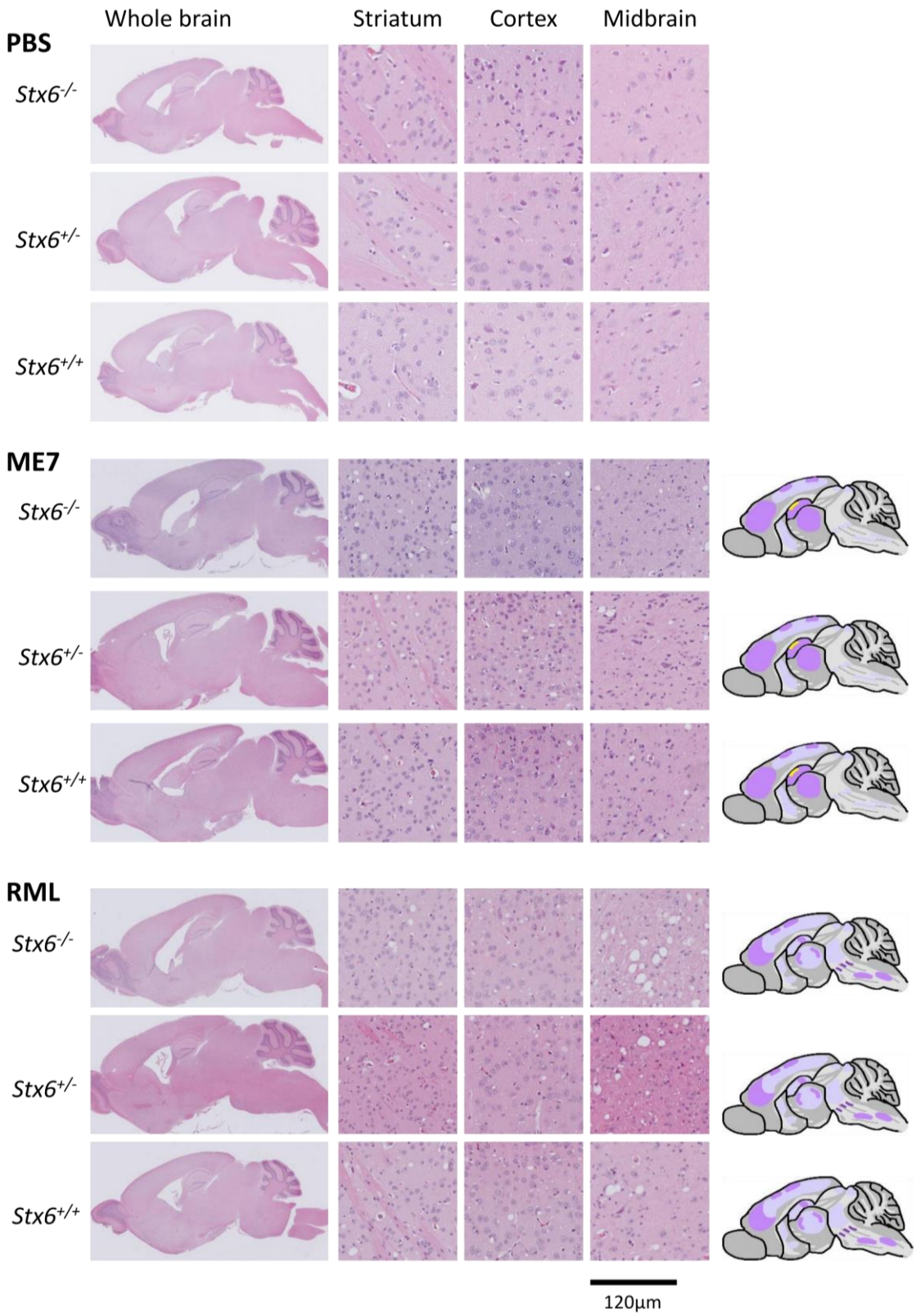

673

674 **Figure 6**

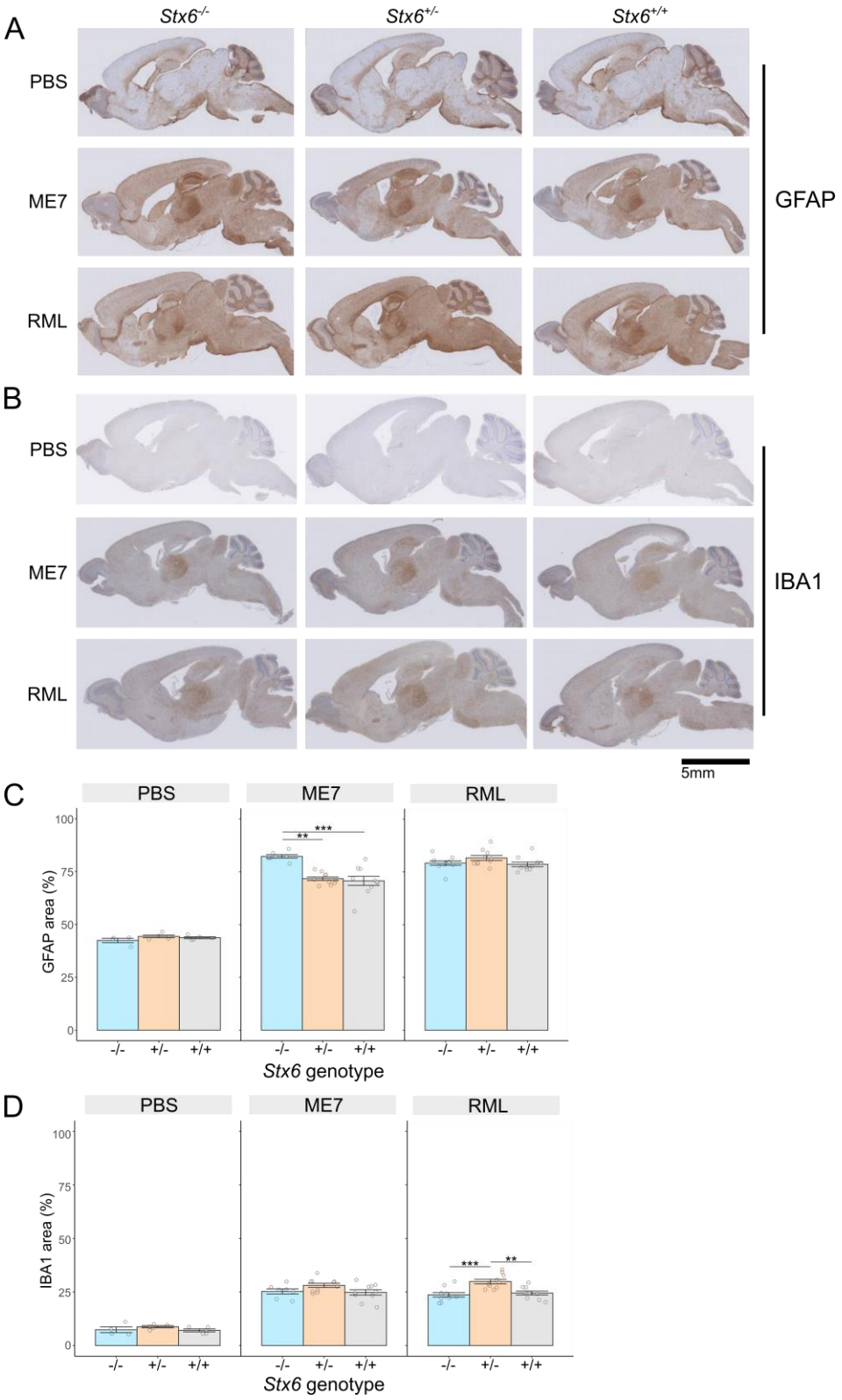

675

676